Bachelor Wiskunde

Track: Biomedische Wiskunde

Bachelor thesis

A mathematical model for calcium dynamics in atrial myocytes

by

Sophia de Jong

July 1, 2016

Supervisor: Dr. R. Planqué

Second examiner: Prof. Dr. D.R.A.W. Notbohm

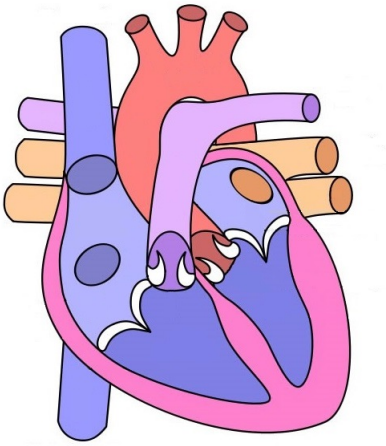

Department of Mathematics
Faculty of Sciences

VU UNIVERSITY AMSTERDAM

Abstract

Atrial fibrillation is the most common arrhythmia, but the process that causes this arrhythmia is unclear. Recently, it has been demonstrated that NAADP-induced calcium release from lysosomes increases the calcium transient amplitude and SR calcium load in atrial myocytes, which can lead to atrial fibrillation. The key question is how NAADP-induced calcium release leads to these results. In this thesis, a mathematical model is developed that describes the dynamics of atrial myocytes. The aim of this thesis is to study how physiological processes and chemical reactions in an atrial myocyte can be translated into mathematics and to get a better understanding of the pathway that causes augmented cellular calcium signals and, possibly, atrial fibrillation. There are multiple theories on how the pathway works. Calcium released from lysosomes could directly influence SERCA or RyR, or could activate CaMKII, which then phosphorylates SERCA or RyR. These four potential processes are modelled and results are generated. The outcomes yield that influence on SERCA is most likely, but the experimentally measured SR load is not reproduced. In future studies, the focus should be on the effect of NAADP-induced calcium release on SERCA.

Title: A mathematical model for calcium dynamics in atrial myocytes
Author: Sophia de Jong, s8.de.jong@student.vu.nl, 2534437
Supervisor: Dr. R. Planqué
Second examiner: Prof. Dr. D.R.A.W. Notbohm
Date: July 1, 2016

Department of Mathematics
Vrije Universiteit Amsterdam
De Boelelaan 1081, 1081 HV Amsterdam
http://www.math.vu.nl/

Contents

1. Introduction

The human heart is divided into left and right halves. Each half consists of an atrium and a ventricle, as is shown in Figure 1.1. During atrial fibrillation, which is the most common arrhythmia, the atria do not synchronically fill the ventricles with blood. This results in a rapid and irregular heart rhythm. Usually, atrial fibrillation episodes do not immediately lead to problems, but in the long run the arrhythmia may lead to other, deathly, diseases. The symptoms of these diseases can be treated, but there does not exist a medicine yet that cures atrial fibrillation, since the process that causes this arrhythmia is unclear.

Myocytes contract upon calcium release from the sarcoplasmic reticulum (SR), the main calcium store in cells. The calcium released from the SR is called the calcium transient. It has been discovered that myocytes also store calcium in lysosomes. Electron micrographs suggest that lysosomes may be strategically located in terms of co-localisation with other calcium related structures such as the SR. The average distance between lysosomes and the SR was measured to be 25 nm (Capel et al., 2015). This has led to the idea that calcium stored in lysosomes may contribute to atrial fibrillation.

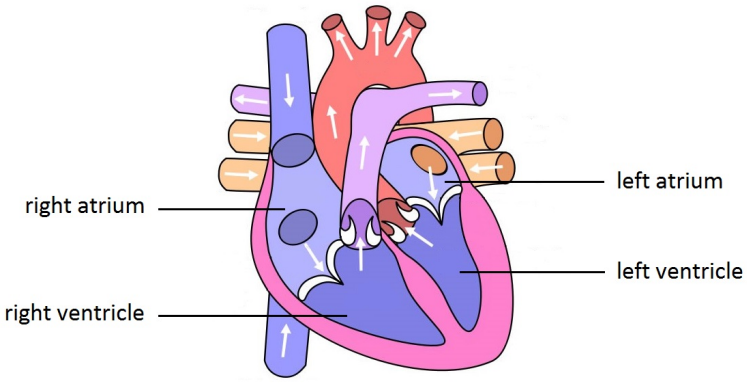

Figure 1.1.: Schematic structure of the heart.

A few years ago, Calcraft et al. (2009) discovered that the calcium signalling second messenger NAADP opens the channel TPC2, which is located on lysosomes. When TPC2s are opened by NAADP, lysosomes release calcium into the cell. This process is called NAADP-induced calcium release. Stimulation of the β-adrenergic receptor activates NAADP-induced calcium release. As a consequence, the force of contraction of the atrial myocyte increases. Long-term, increased calcium signalling is a known causative

factor for the development of atrial fibrillation. Nevertheless, the precise events that are involved, including a possible contribution of the NAADP pathway, remain unclear.

Dr. Rebecca A. Capel and Dr. Rebecca B. Burton from the University of Oxford investigate atrial fibrillation. In their latest paper, *TPC2 and NAADP enhance cardiac β-adrenoceptor signaling* (Capel et al., 2015), they demonstrate that mice lacking the lysosomal calcium release protein TPC2 are protected from ventricular hypertrophy and arrhythmias. Their data indicate that NAADP acts in atrial myocytes to increase the size of the calcium transient and that it no longer acts in the presence of a specific NAADP inhibitor.

Dr. Rebecca A. Capel and Dr. Rebecca B. Burton visited the Vrije Universiteit Amsterdam in February. I met with them and they explained what they know about NAADP-induced calcium release and what they would like to find out. Lysosomal calcium signalling is a little-studied pathway in the heart which has been implicated in the adrenergic responses of both atrial (Collins et al. 2011) and ventricular myocytes (Bayliss et al. 2012). Recently, Capel et al. (2015) found that stimulation of the β-adrenoceptor on the cell membrane increases the calcium transient amplitude and SR calcium load. The NAADP pathway forms part of this response and has not been studied very much in the heart. They hope that a mathematical model will help to gain insight in the pathway that causes these results. The key question is how NAADP-induced calcium release from lysosomes leads to an increased calcium transient amplitude and SR calcium load.

There are multiple potential answers to this question. Among them is the option that calcium released from lysosomes is immediately transferred into the SR by the protein SERCA. This could explain the increased calcium transient and SR load. Another theory is that the released calcium acts on RyR. This receptor releases calcium from the SR. But calcium does not have to influence the SR directly. Calcium could also activate other substances which then increase the calcium transient and SR load. One of these substances is CaMKII. This protein is activated by calcium and can phosphorylate other proteins, thereby increasing their activity. It has been shown that application of NAADP does not result in an increased calcium transient when CaMKII is inhibited (Capel et al., 2015). This leads to two more options. The third option is phosphorylation of SERCA by CaMKII. The fourth and last option I will examine, is phosphorylation of RyR by CaMKII. This could result in a higher calcium transient amplitude and SR calcium load.

The question cannot be answered by biomedical experiments only, since concentrations and activities of the proteins involved are hard, if not impossible, to measure. To gain insight in the dynamics of NAADP-induced calcium release and the increased calcium transient and SR load, I have developed mathematical models for the four theories. I started with an already existing model that describes the calcium dynamics of the atrial myocyte under normal circumstances. This model has been developed by Grandi et al. (2011). I have added NAADP-induced calcium release to this model. I then separately

modelled each of the four processes that are possibly involved in increasing the calcium transient and SR load. The differential equations of the model were numerically solved in MATLAB®.

The aim of this thesis is to get a better understanding of the pathway that causes augmented cellular calcium signals and, possibly, atrial fibrillation, and to study how physiological processes and chemical reactions in an atrial myocyte can be translated into mathematics. In Chapter 2, the processes and proteins involved in the contraction of myocytes and atrial fibrillation are explained in more detail. Chapter 3 describes the model developed by Grandi et al. (2011). The compartments of the model are explained and the model equations are considered. I extend this model in Chapter 4. The first part of this chapter describes how NAADP-induced calcium release is modelled and the second part describes the models for the four processes that could increase the calcium transient and SR load. Results are generated in Chapter 5. To conclude, the results are discussed and the model is reviewed in Chapter 6.

2. Cardiac physiology

The heart consists of muscle cells named cardiac myocytes. Myocytes contract after being excited by an action potential. An action potential is a short event in which the membrane potential rapidly increases and decreases. The cell membrane, or sarcolemma, contains several voltage-gated ion channels, which open and close at different values of the membrane potential, transporting ions through the sarcolemma and thereby allowing action potentials to occur. Calcium ions play a major role in the contraction of myocytes. Figure 2.1 provides an overview of the processes described in this chapter.

2.1. Calcium-induced calcium release

Cardiac myocytes contain a sarcoplasmic reticulum (SR). The SR is a calcium (Ca^{2+}) store. The protein sarco/endoplasmic reticulum Ca^{2+}-ATPase (SERCA) transfers calcium from the cytosol to the SR. SERCA pumps more calcium across the SR membrane per unit time when the calcium concentration in the cytosol rises, resulting in a higher SR load, which decreases the activity of SERCA again. The protein phospholamban (PLB) is positioned around SERCA, decreasing its activity in the normal unphosphorylated state. When PLB is phosphorylated, its conformation changes and the activity of SERCA increases.

L-type calcium channels are positioned on the sarcolemma and are located close to the SR. These channels open upon depolarisation of the sarcolemma. This results in a flow of calcium ions into the cell. Ryanodine receptors (RyRs) are positioned on the SR, close to the L-type calcium channels. RyR has activating binding sites and slower inactivating binding sites for calcium in the cytosol. The small influx of calcium through L-type calcium channels activates RyR, resulting in a large calcium release from the SR. This positive feedback mechanism is called calcium-induced calcium release. Eventually this leads to negative feedback, since the inactivating calcium binding sites become occupied, inhibiting RyR to release calcium from the SR. RyR also has an activating calcium binding site located inside the SR. When calcium binds to this site, the affinity of the cytosolic activating site increases, whereas the affinity of the inactivation site decreases. In this complicated way, the calcium concentration in the SR influences the release by RyR (Shannon et al., 2004).

2.2. NAADP-induced calcium release

Over the last fifteen years, the concept of nicotinic acid adenine dinucleotide phosphate (NAADP) as part of the β-adrenergic pathway in the heart has been established. The principal process driving contraction of cardiac myocytes is calcium-induced calcium release, but β-adrenergic stimulation increases the heart rate and force by raising the amplitude of the calcium transient. The β-adrenoceptor is located on the sarcolemma and is regulated by the extracellular environment. Stimulation of this receptor leads to stimulation of adenylyl cyclase which forms cyclic AMP. This substance in turn activates PKA, which then phosphorylates a family of multi-functional enzymes termed ADP-ribosyl cyclases. These enzymes have been suggested to synthesise NAADP (Aarhus et al., 1995). In short, β-adrenergic stimulation increases the concentration of NAADP.

Studies have shown that NAADP is involved in increasing the calcium transient amplitude (Capel et al., 2015). The effects of NAADP were associated with an increase in the SR calcium load (Collins et al., 2011). Lysosomes are thought to be involved in this process. The receptor for NAADP in atrial myocytes has been identified as being two-pore channel type 2 (TPC2) (Calcraft et al., 2009). TPCs are exclusively expressed on vacuolar or lysosomal membranes. There are three TPC types, of which TPC2 releases calcium from lysosomes. The lysosomal calcium release resulting from opening TPC2 by NAADP is called NAADP-induced calcium release (Capel et al., 2015). In Figure 2.1, this process is schematically presented. The concentration of NAADP that is necessary for opening TPC2 is limited. When the NAADP concentration is too high, the open probability of the channel decreases. This is a self-inactivating system for high concentrations of NAADP (Pitt et al., 2010).

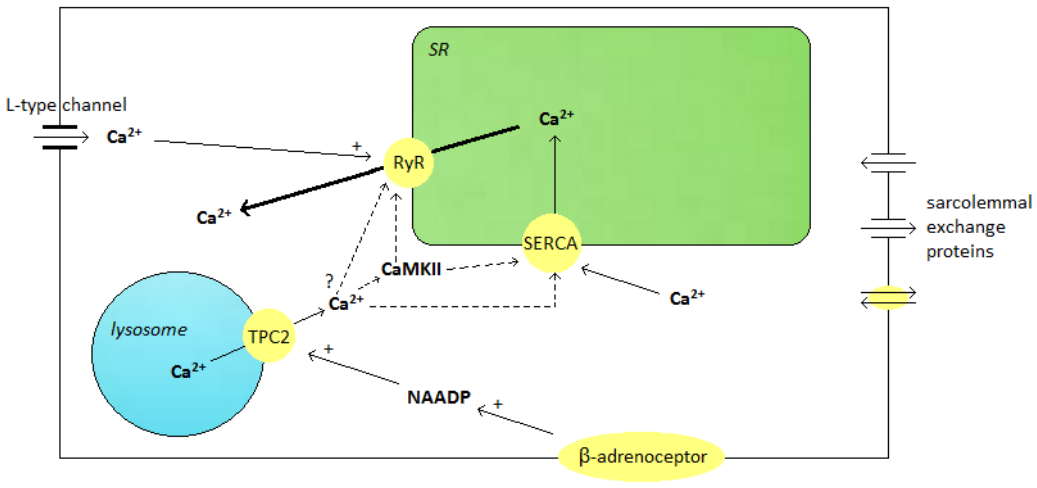

Figure 2.1.: Calcium-induced calcium release and NAADP-induced calcium release. The dotted lines represent the four possible mechanisms that could lead to an increase in the calcium transient amplitude and SR calcium load upon β-adrenergic stimulation.

It is unclear how NAADP-induced calcium release increases the calcium transient amplitude and SR calcium load. The amount of calcium released from lysosomes is too small to make a difference in the cytosolic calcium concentration (Dr. R.A. Capel). Hence, lysosomal calcium release must indirectly increase the calcium transient.

Lysosomes were observed close to the SR. Figure 2.2 shows an electron micrograph of a part of a cardiac myocyte. The average distance between lysosomes and the SR has been estimated to be 25 nm (Capel et al., 2015). This small space between lysosomes and the SR is called the nanojunction and has been described by Helle et al. (2013). When lysosomes release calcium ions, these ions could be taken up into the SR by SERCA, increasing the SR calcium load, or these ions could influence RyR. This could enhance the activity of RyR and explain the increased calcium transient. But it also has been hypothesised that activation of calcium/calmodulin-dependent protein kinase II (CaMKII) gives rise to phosphorylation within the cardiac myocyte. High concentrations of calcium and calmodulin activate CaMKII. When lysosomes locally release calcium, this could activate CaMKII, leading to the phosphorylation of PLB, which is bound to SERCA, or RyR or both, resulting in an increased calcium transient (Capel et al., 2015) . Figure 2.1 provides an overview of calcium-induced calcium release, NAADP-induced calcium release and the four possible processes.

The experiments in Capel et al. (2015) suggest that β-adrenergic stimulation gives rise to NAADP-induced calcium release from lysosomes into the nanojunction, but it is not known how lysosomal calcium release leads to the observed increased calcium transient amplitude and SR calcium load. This thesis aims to provide insight in the mechanism that leads to these results.

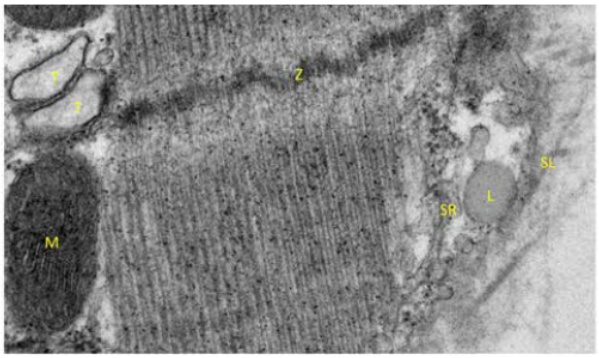

Figure 2.2.: Electron micrograph showing the subcellular relationships of cardiac lysosomes in rabbit. A lysosome (L) is closely apposed to the SR. The sarcolemma (SL), a mitochondria (M) and a Z-line can also be seen. Contraction proteins are bound to the Z-line. This is Figure 5A of Capel et al. (2015).

3. A human atrial action potential model

The dynamics of the heart have been modelled by many researchers. Over the years, these models have been improved. Grandi et al. (2011) have created a detailed human atrial action potential model. This model describes several ion currents and the resulting membrane potential and calcium transient in atrial myocytes under normal circumstances. The original model was made by Shannon et al. (2004). This model describes the dynamics of ventricular myocytes in rabbits. Mainly by replacing parameters, Grandi et al. (2011) fitted the model to the results from their human atrial myocyte experiments. I refer to the data supplement of Grandi et al. (2011) for the parameter values that are used.

The human atrial action potential model developed by Grandi et al. (2011) is composed of thirty-nine differential equations. The differential equations describe the concentrations of calcium (Ca^{2+}), sodium (Na^{+}), potassium (K^{+}) and chloride (Cl^{-}) ions and the dynamics of ion channels and other exchange proteins in the cell. The membrane potential is reconstructed from the ion currents through the sarcolemmal membrane channels. After disturbance of cellular concentrations, the solutions of the model always return to steady state. First I will provide an overview of the structure of the model by defining the compartments and describing the equations that establish the membrane potential. Since calcium is the leading ion in generating myocyte contraction, I will then discuss the dynamics of SERCA and RyR and focus on the differential equations describing calcium dynamics.

3.1. The compartments of the model

The atrial myocyte has been divided by Shannon et al. (2004) into four compartments, namely, SR, junction, SL and bulk cytosol. This is shown in Figure 3.1. The junction is a small space between the sarcolemma and the SR. In this space, L-type calcium channels and RyRs are in close contact. It is assumed that the junction accounts for 11% of the whole space just beneath the sarcolemma and 90% of the L-type channels are located in the junction, while all other channels are evenly distributed throughout the cell membrane. The remaining 89% cytosol beneath the sarcolemma is called the SL. Shannon et al. (2004) have introduced this compartment since ion concentrations measured near the sarcolemma were found to differ from those measured elsewhere in the cell. This is likely due to diffusion restrictions caused by large organelles in the cell,

such as mitochondria. Due to the SL compartment, the model better accounts for the activity of the sarcolemmal membrane channels than previous models. The remaining cytosol of the cell is called the bulk cytosol.

Ions can freely diffuse between the compartments. The junction is adjoined to the SL and the SL is adjoined to the bulk cytosol. All RyR proteins are positioned on the side of the SR that is next to the junction. Hence, calcium released from the SR flows into the junction. The SERCA proteins are located next to the bulk cytosol, so calcium uptake occurs there. Figure 3.1 provides an overview of the four compartments of the model and the most important exchange proteins.

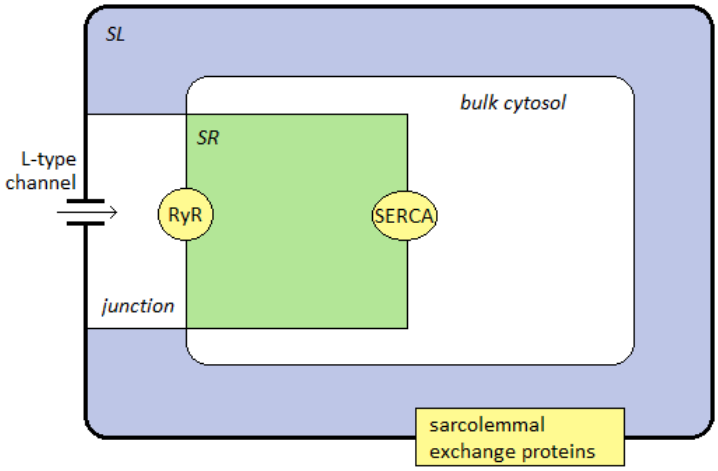

Figure 3.1.: The compartments of the model as defined by Shannon et al. (2004).

3.2. Sarcolemmal exchange proteins

Many ions are exchanged through the sarcolemma using several ion channels and protein pumps, which all differ in permeability and open probability. The states of these channels are dependent on the membrane potential. The membrane potential is determined by the ion currents through the sarcolemma, which depend on the ion concentrations and the states of the ion channels. Ion channels can be modelled in various ways.

3.2.1. The membrane potential

The capacitance of the cell membrane is defined by

$$C_m = \frac{Q}{V_m},$$

where Q is the charge across the membrane and V_m is the membrane potential required to hold the charge. The total ion current I_{tot} through the cell membrane is equal to $\frac{dQ}{dt}$.

It follows that the membrane potential can be described by

$$\frac{dV_m}{dt} = \frac{I_{tot}}{C_m}.$$

The total ion current consists of the currents through all ion channels at time t. This current can be described by

$$I_{tot} = Ng(V_m, t)\phi(V_m),$$

where there are N channels positioned on the membrane, $g(V_m, t)$ is the fraction of open channels at time t and membrane potential V_m, and $\phi(V_m)$ describes how the current through one open channel depends on the membrane potential (Diekmann and Planqué, 2014). However, the definitions for g and ϕ highly differ for various ion channels. In the model of Grandi et al. (2011), the total ion current is defined by the sum of all ion currents that pass through the cell membrane by different ion channels.

3.2.2. The Nernst potential

The simplest way to define ϕ is to assume that the ion current depends linearly on the membrane potential and is zero at a particular value of the membrane potential, called the Nernst potential. The Nernst potential for a channel for ion X is defined by

$$V_{NX} = \frac{RT}{zF} \log\left(\frac{[X]_e}{[X]_i}\right), \tag{3.1}$$

where $[X]_i$ and $[X]_e$ are the concentrations of ion X in the intracellular and extracellular compartment respectively, R is the universal gas constant, T is the temperature in degrees Celsius, z is the charge on ion X and F is Faraday's constant (Keener and Sneyd, 2009). The function ϕ for a channel for ion X can in this case be defined by

$$\phi(V_m) = V_m - V_{NX}. \tag{3.2}$$

In the model of Grandi et al. (2011), the background currents of calcium, sodium and chloride are linearly dependent on the Nernst potentials for these ions. Since the cytosol beneath the sarcolemma is divided into the junction and the SL, the ion currents through each type of channel are distinguished. For instance, the background calcium current is described by

$$\begin{aligned} I_{Cabkjunc} &= F_{junc}\, G_{Cabk}\left(V_m - V_{NCa_j}\right), \\ I_{CabkSL} &= F_{SL}\, G_{Cabk}\left(V_m - V_{NCa_{SL}}\right), \\ I_{Cabk} &= I_{Cabkjunc} + I_{CabkSL}, \end{aligned}$$

whereby G_{Cabk} is constant. The parameters $F_{junc} = 0.11$ and $F_{SL} = 0.89$ define the division of the cytosol beneath the sarcolemma into the junction and SL. The ion currents depend on the Nernst potentials for calcium in the junction, V_{NCa_j}, and calcium in the SL, $V_{NCa_{SL}}$, which are dynamic. Henceforth, I will not make the distinction between ion currents in the junction and SL. The ion current through a sarcolemmal ion channel is always described by the sum of that current in the junction and the SL.

3.2.3. Two-state model

Ion channels can have multiple gates. In general, a channel is assumed to be open if all its gates are open. Consider a channel with only one gate. Let R denote the resting state of the channel and let O denote the open state. The fraction of open channels g changes according to the reaction scheme

$$R \underset{b}{\overset{a}{\rightleftharpoons}} O,$$

where the rates a and b are dependent on the membrane potential V_m. This can be described by the differential equation

$$\frac{dg}{dt} = a(1-g) - bg. \tag{3.3}$$

This results in a fraction of $g = \frac{a}{a+b}$ open channels in steady state (Diekmann and Planqué, 2014).

Grandi et al. (2011) have defined the fraction of open channels for the inward rectifier potassium channel as in Equation 3.3. This channel transfers potassium out of the cell, establishing the resting membrane potential of -85 mV. This channel should not be confused with the potassium channels that transfer potassium out of the cell after depolarisation. The inward rectifier potassium channel closes during depolarisation. If it was always open, it would be almost impossible to stimulate an action potential. The inward rectifier potassium channel depends on the membrane potential and the extracellular potassium concentration. The rates a and b are defined by

$$a_{KI} = \frac{1.02}{1 + \exp\left(0.24\left(V_m - 59.22 - V_{NK}\right)\right)},$$

$$b_{KI} = \frac{0.49\exp\left(0.08\left(V_m + 5.48 - V_{NK}\right)\right) + \exp\left(0.06\left(V_m - 594.31 - V_{NK}\right)\right)}{1 + \exp\left(-0.51\left(V_m + 4.75 - V_{NK}\right)\right)}.$$

The Nernst potential V_{NK} for potassium ions is described by Equation 3.1 and is constant, since the intracellular and extracellular potassium concentrations are assumed to be constant. Figure 3.2 shows that a_{KI} rapidly decreases when V_m exceeds 10 mV, while b_{KI} starts to increase at that point. So when the membrane depolarises, the inward rectifier potassium channels close. Other channels transfer potassium out of the cell, causing repolarisation. As a result, the inward rectifier potassium channels open again and establish the resting membrane potential.

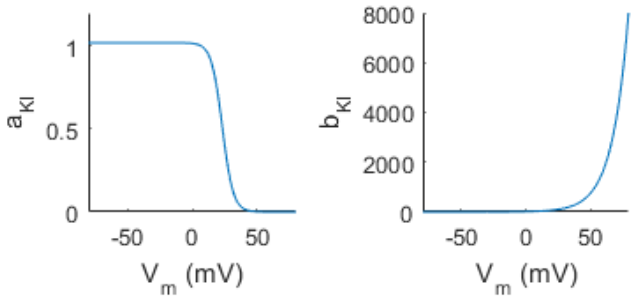

Figure 3.2.: The dependence of the rates of the two-state model for the inward rectifier potassium channel on the membrane potential.

The inward rectifier potassium current can now be described by

$$I_{KI} = 0.35\sqrt{\frac{K_o}{5.4}}\,\frac{a_{KI}}{a_{KI}+b_{KI}}\,(V_m - V_{NK})\,,$$

where K_o is the constant extracellular potassium concentration and V_{NK} is the Nernst potential for potassium ions.

3.2.4. Activation time constants

Many ion channels have different reaction times for changes in the membrane potential. The occurrence of an action potential is due to the fact that sodium channels open and close fast. Potassium channels are relatively slow. The dynamics of these channels can be modelled using time constants. Consider Equation 3.3 again. This equation can be rewritten as

$$\tau_g \frac{dg}{dt} = \frac{a}{a+b} - g, \tag{3.4}$$

to emphasise that the fraction of open channels g converges to $\frac{a}{a+b}$ at the time scale τ_g (Diekmann and Planqué, 2014).

The transient outward potassium channel, responsible for repolarisation, is described by Grandi et al. (2011) using time constants. The channel is activated rapidly upon depolarisation, but is inactivated more slowly. The steady state equations for activation and inactivation are respectively defined by

$$x_{toss} = \frac{1}{1+\exp\left(-\frac{V_m+1}{11}\right)},$$
$$y_{toss} = \frac{1}{1+\exp\left(\frac{V_m+40.5}{11.5}\right)},$$

and are pictured in the left plot of Figure 3.3. It can be seen that the channel becomes activated for high values of the membrane potential, or in other words, during depolarisation. As a result, potassium ions are transferred out of the cell and the membrane

repolarises, leading to inactivation of the channel. To make sure that activation is faster than inactivation, time constants

$$\tau_{xto} = 3.5 \exp\left(-\left(\frac{V_m}{30}\right)^2\right) + 1.5,$$
$$\tau_{y_{to}} = 25.6 \exp\left(-\left(\frac{V_m + 52.5}{15.9}\right)^2\right) + 24.1,$$

are defined. The right plot of Figure 3.3 shows the dependence of these time constants on the membrane potential. It is clear that τ_{xto} is always smaller than $\tau_{y_{to}}$, so activation is always faster. When the membrane depolarises, τ_{xto} increases and hence activation of the channel is slightly slowed down. However, when the membrane potential becomes positive, the activation rate increases again. When the membrane repolarises, $\tau_{y_{to}}$ increases, so inactivation of the channel gets restrained, until the potential reaches below -50 mV. This ensures slow inactivation upon repolarisation.

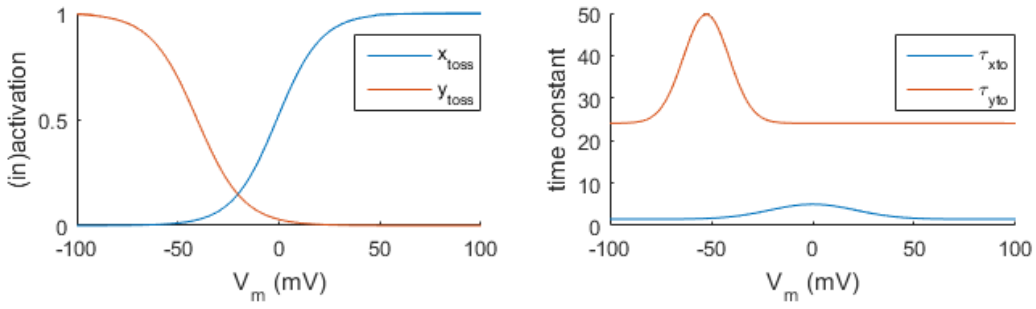

Figure 3.3.: The dependence of the activation and inactivation fractions and time constants on the membrane potential.

Like in Equation 3.4, the differential equations for activation and inactivation of the transient outward potassium channel are described by

$$\frac{dx_{to}}{dt} = \frac{x_{toss} - x_{to}}{\tau_{xto}},$$
$$\frac{dy_{to}}{dt} = \frac{y_{to_{ss}} - y_{to}}{\tau_{y_{to}}}.$$

The transient outward potassium current can now be described by the equation

$$I_{to} = G_{to}\, x_{to}\, y_{to}\, (V_m - V_{NK}),$$

where G_{to} is constant and V_{NK} is the Nernst potential for potassium ions.

3.2.5. Allosteric regulation

Many channels do not only depend on the membrane potential, but are also allosterically regulated. This is often described as follows. Consider the chemical equation

$$X + R \underset{k_-}{\overset{k_+}{\rightleftharpoons}} O.$$

Ion X binds to channel R, which is in the resting state, and this results in a transition of the channel to the open state O with rate k_+. The complex can fall apart again with rate k_-. Under the assumption that the total number of ion channels, $R_T = R + O$, is constant, the dynamics of the channel can be described by the differential equation

$$\frac{dO}{dt} = k_+ \left(R_T - O\right) X - k_- O.$$

The steady state solution of this equation is

$$O = R_T \frac{X}{K_D + X}, \tag{3.5}$$

whereby $K_D = \frac{k_-}{k_+}$ is called the dissociation or half-saturation constant. The affinity of the channel R for the ion X can be considered as $\frac{1}{K_D}$ (Bruggeman, 2014).

The Ca^{2+}-activated Cl^- channel is sensitive to the membrane potential and the intracellular calcium concentration. When the channel is open, chloride ions are transferred through the sarcolemma. The channel is modelled by Grandi et al. (2011) according to Equations 3.2 and 3.5. The resulting equation for the ion current is

$$I_{ClCa} = G_{ClCa} \frac{Ca}{K_{DClCa} + Ca} \left(V_m - V_{NCl}\right),$$

whereby G_{ClCa} is constant, Ca is the calcium concentration in the junction or SL and V_{NCl} is the Nernst potential for chloride ions, described by Equation 3.1. The Nernst potential is constant, since the intracellular and extracellular chloride concentrations are assumed to be constant.

For many reactions, the affinity of the channel for an ion does not follow a simple hyperbolic curve, as in model above, but often follows a sigmoid curve. This can be due to cooperativity. An ion channel can be bound by multiple ions and the number of ions bound to the channel can affect the conformation of the channel, resulting in a different ion affinity. The binding of n ions X to a channel R can be described by the reaction scheme

$$nX + R \underset{k_-}{\overset{k_+}{\rightleftharpoons}} R_{Xn}.$$

This results in the differential equation

$$\frac{dR_{Xn}}{dt} = k_+ \left(R_T - R_{Xn}\right) X^n - k_- R_{Xn},$$

which describes the dynamics of the channel R_{Xn}, which is bound by n ions X. The steady state solution of this differential equation is

$$R_{Xn} = R_T \frac{X^n}{K_{0.5}^n + X^n},$$

where $K_{0.5} = \sqrt[n]{\frac{k_-}{k_+}}$ is the concentration of ions X where half of the channels R are bound by n ions X. This equation is called the Hill equation (Weiss, 1997). However, the ligand binding mechanism reflected by the Hill equation is not physically possible, except for $n = 1$. For higher values of n, the equation implies that multiple ions bind to the channel at the exact same time. That means that there are no states of the channel in between R and R_{Xn}. Hence, the Hill equation is just an easy way to model cooperativity and the Hill coefficient n is better thought of as an interaction coefficient that an estimation of the number of binding sites on the channel. The Hill equation can also take decimal values, if that fits the data best.

The Ca^{2+}-ATPase is modelled using the Hill equation. This protein removes calcium from the cell. Its activity depends on the calcium concentration inside the cell. In the model of Grandi et al. (2011), the Ca^{2+}-ATPase current is described by

$$I_{pCa} = \bar{I}_{PMCA} \frac{Ca^{1.6}}{{K_{0.5pCa}}^{1.6} + Ca^{1.6}},$$

where $\bar{I}_{PMCA}$ is the maximal calcium current through the Ca^{2+}-ATPase and $K_{0.5pCa}$ is the calcium concentration Ca for which the calcium current is half-maximal.

The other sarcolemmal ion currents that contribute to the membrane potential are described by a combination of the models above. I refer to the data supplement of Grandi et al. (2011) for the equations that define these currents.

3.3. SERCA dynamics

Calcium in the bulk cytosol is transferred into the SR by SERCA. This is a reversible enzyme, which means that calcium can be transferred in both directions across the SR membrane. Nevertheless, in the model of Grandi et al. (2011) the net SERCA rate never reverses and is always directed into the SR. The rate depends on the calcium concentration in the SR (Ca_{SR}) and the bulk cytosol (Ca_i). During calcium release from the SR, Ca_i rises and Ca_{SR} falls. This stimulates SERCA to transport more calcium into the SR. As a consequence, Ca_{SR} rises and Ca_i falls, decreasing the rate of uptake.

In the model of Grandi et al. (2011), the calcium flux through SERCA is described by the Hill equation

$$J_{SERCA} = V_{max_{SERCA}} \frac{\left(\frac{Ca_i}{Km_f}\right)^H - \left(\frac{Ca_{SR}}{Km_r}\right)^H}{1 + \left(\frac{Ca_i}{Km_f}\right)^H + \left(\frac{Ca_{SR}}{Km_r}\right)^H}. \tag{3.6}$$

The value of Km_f is 3000 times smaller than Km_r. This ensures that J_{SERCA} is positive under normal circumstances, such that calcium is taken up and not released by SERCA.

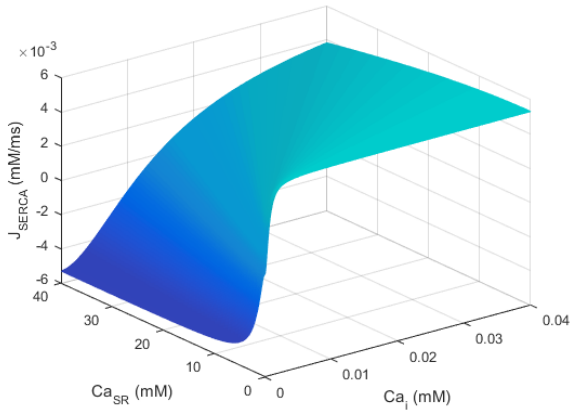

Figure 3.4.: The dependence of J_{SERCA} on Ca_i and Ca_{SR}.

The flux through SERCA is plotted against Ca_i and Ca_{SR} in Figure 3.4. It is clear that J_{SERCA} increases when Ca_i rises. The maximal flux is reached faster when Ca_{SR} is small. As long as Ca_i is higher than

$$\frac{Km_f}{Km_r} Ca_{SR},$$

J_{SERCA} is positive and Ca_i will be transported into the SR. The Hill coefficient H determines the slope of the function. Higher values of H result in a larger slope. The slope is also highly affected by Km_f. Decreasing Km_f leads to a larger slope.

3.4. RyR dynamics

In the model of Grandi et al. (2011), it is assumed that RyR has four states. The protein can be resting (R), open (O), inactivated (I) or resting inactivated (RI). Upon depolarisation and calcium influx through L-type channels, junctional calcium (Ca_j) binds to the activation site on RyR. This results in a transition from the resting to the open state. At the same time, calcium ions bind to slower inactivation sites, which leads to a transition to the inactivated state. As calcium declines, there is a transition to the resting inactivated state. This means that calcium is no longer bound to the inactivation sites, but the receptor remains inactivated. Eventually, RyR returns to the resting state. Only RyRs that are in the open state can transfer calcium from the SR to the junction. The dynamics of RyR can be described by the system of differential equations

$$\begin{aligned} RI &= 1 - R - O - I, \\ \frac{dR}{dt} &= (ki_m RI - ki_{SR_{Ca}} Ca_j R) - (ko_{SR_{Ca}} {Ca_j}^2 R - ko_m O), \\ \frac{dO}{dt} &= (ko_{SR_{Ca}} {Ca_j}^2 R - ko_m O) - (ki_{SR_{Ca}} Ca_j O - ki_m I), \\ \frac{dI}{dt} &= (ki_{SR_{Ca}} Ca_j O - ki_m I) - (ko_m I - ko_{SR_{Ca}} {Ca_j}^2 RI). \end{aligned} \tag{3.7}$$

Hence, in the model RyR transits from the resting to the open state when it is bound to two junctional calcium ions. When a third calcium ion binds to RyR, there is a transition from the open to the inactivated state.

The states are also dependent on the concentration of calcium inside the SR. When calcium binds to the activation site on the inside of the SR, the affinity of the activation site on the outside increases whereas the affinity of the inactivation site decreases. This results in a greater tendency for RyR to transit to the open state. This is modelled by making $ko_{SR_{Ca}}$ and $ki_{SR_{Ca}}$ dependent on Ca_{SR}. By defining

$$\begin{aligned} ko_{SR_{Ca}} &= ko_{Ca} \frac{{Ca_{SR}}^{2.5} + ec}{{Ca_{SR}}^{2.5} + 15ec}, \\ ki_{SR_{Ca}} &= ki_{Ca} \frac{{Ca_{SR}}^{2.5} + 15ec}{{Ca_{SR}}^{2.5} + ec}, \end{aligned} \tag{3.8}$$

the tendency increases to transit from the resting to the open state when the calcium load of the SR is higher, since $ko_{SR_{Ca}}$ is an increasing function. There also is less tendency to transit from the open to the inactivated state and from the resting to the resting inactivated state, since $ki_{SR_{Ca}}$ decreases, but there is a greater tendency to transit from the resting inactivated to the inactivated state. This gives rise to a higher fraction of open RyRs in steady state.

For fixed calcium concentrations, Equations 3.7 form a linear homogeneous system. Hence, the steady state equations of this system can be calculated analytically for fixed

calcium concentrations. The open probability equals the fraction of RyRs in the open state. Its steady state equation is

$$O = \frac{ki_m}{ki_{SR_{Ca}}\left(Ca_j + \frac{ki_m}{ki_{SR_{Ca}}} + \frac{ko_m}{Ca_j ko_{SR_{Ca}}} + \frac{ki_m ko_m}{{Ca_j}^2 ki_{SR_{Ca}} ko_{SR_{Ca}}}\right)}.$$

The open probability is plotted against the junctional calcium concentration in Figure 3.5. The maximal value of the open probability is 0.0014 and this is reached when the junctional calcium concentration is 0.28 mM. Under normal circumstances, this concentration fluctuates around 0.03 mM. Hence, the open probability of RyR only decreases when extremely high concentrations of calcium are reached.

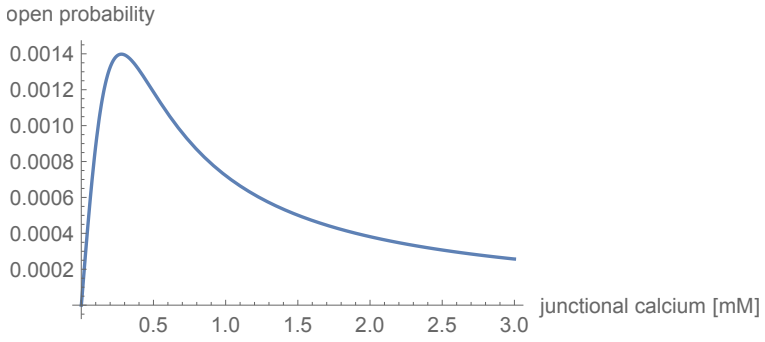

Figure 3.5.: The open probability of RyR against the junctional calcium concentration.

The junctional calcium concentration for which the maximal open probability of RyR is reached, depends on ki_m, ko_m, $ki_{SR_{Ca}}$ and $ko_{SR_{Ca}}$. This concentration increases when ki_m and ko_m increase or $ki_{SR_{Ca}}$ and $ko_{SR_{Ca}}$ decrease. Changes in ko_m or $ko_{SR_{Ca}}$ are more effective.

The calcium current through RyR can now be described by

$$J_{RyR} = k_s \; O \; (Ca_{SR} - Ca_j).$$

This current will always be positive in this model, because the calcium concentration in the SR is always higher than the calcium concentration in the junction. In addition, if the junctional concentration would exceed the SR calcium load, all RyRs would close and hence the flux would equal zero. Also due to this high difference in calcium concentration, the SR always leaks small amounts of calcium into the junction,

$$J_{SR_{leak}} = D_{leak} \; (Ca_{SR} - Ca_j).$$

3.5. Calcium dynamics

The differential equations for the changes in the concentration of calcium in the four compartments can now be defined. Apart from the calcium exchange with other compartments, calcium ions are buffered by large proteins. In fact, the majority of calcium is buffered, with only little in the form of free calcium ions. Differential equations are defined for each substance that buffers calcium. In total, there are twelve differential equations that describe the activity of calcium buffers and two that describe the activity of sodium buffers. I will not write out all equations in detail. Instead, I give the form of the differential equation of an ion A to bind to a buffer B such that the complex A_B is formed. This can be described by

$$\frac{dA_B}{dt} = k_{on} A \left(B_{max} - A_B\right) - k_{off} A_B,$$

whereby B_{max} is the maximal buffer capacity of buffer B, and k_{on} and k_{off} are the rate coefficients for the complex to form and collapse respectively. I refer to the data supplement of Grandi et al. (2011) for the detailed equations.

The equations below describe the dynamics of the calcium concentrations in the four compartments. Figure 3.1 provides an overview of the compartments of the myocyte.

The bulk cytosol exchanges calcium with the SL and calcium in the bulk cytosol is transferred to the SR by SERCA. This can be described by the differential equation

$$\frac{dCa_i}{dt} = -J_{SERCA} \frac{V_{SR}}{V_{bulk}} + \frac{D_{SLbulk}}{V_{bulk}}(Ca_{SL} - Ca_i) - J_{Bbulk},$$

whereby V_{SR} and V_{bulk} are the volumes of the SR and bulk cytosol, D_{SLbulk} is a measure for the diffusion between the SL and bulk cytosol compartments, Ca_{SL} is the calcium concentration in the SL, and J_{Bbulk} is the equation that describes the buffering of cytosolic calcium.

The SR receives calcium from the bulk cytosol by SERCA and releases calcium into the junction by RyR activity and calcium leak. This is defined by

$$\frac{dCa_{SR}}{dt} = J_{SERCA} - J_{RyR} - J_{SRleak} \frac{V_{bulk}}{V_{SR}} - J_{Bsr},$$

where J_{Bsr} is the equation for buffered calcium in the SR.

The junction exchanges calcium with the extracellular environment and the SL compartment, and receives calcium from the SR by RyR activity and calcium leak. The equation

$$\frac{dCa_j}{dt} = -J_{exjunc} \frac{C_m}{2F\ V_{junc}} + \frac{D_{SLjunc}}{V_{junc}}(Ca_{SL} - Ca_j) + J_{RyR} \frac{V_{SR}}{V_{junc}} + J_{SRleak} \frac{V_{bulk}}{V_{junc}} - J_{Bj},$$

describes this process. The flux J_{exjunc} comprises all calcium exchange through sarcolemmal ion channels and pumps. The parameter C_m is the capacitance of the sarcolemma and F is the Faraday constant. The junctional volume is denoted by V_{junc} and D_{SLjunc} is a measure for the diffusion between the SL and the junction. The equation J_{Bj} takes into account all calcium buffer activity in the junction.

The SL exchanges calcium with the extracellular environment, the junction and the bulk cytosol, according to the equation

$$\frac{dCa_{SL}}{dt} = -J_{exSL}\,\frac{C_m}{2F\;V_{SL}} + \frac{D_{SLjunc}}{V_{SL}}\,(Ca_j - Ca_{SL}) + \frac{D_{SLbulk}}{V_{SL}}\,(Ca_i - Ca_{SL}) - J_{Bsl},$$

where J_{exSL} takes into account all calcium exchange with the extracellular environment and J_{Bsl} denotes the equation for buffered calcium in the SL.

Figure 3.6 illustrates the development of the calcium concentrations in the four compartments. The junctional calcium concentration peaks first and the concentration in the SR decreases. As a result, the junctional concentration further increases. The concentrations in the bulk cytosol and SL follow, due to diffusion. These concentrations reach lower maxima since these compartments have greater volume. This all happens in the first 80 ms. The myocyte then returns to its resting state.

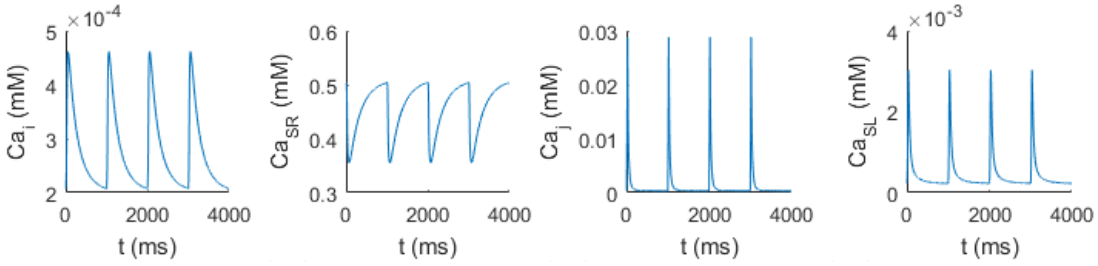

Figure 3.6.: The concentrations of calcium in the four compartments during four heartbeats.

4. Modelling NAADP-induced calcium release

I have extended the model of Grandi et al. (2011) in the following way. First, I defined the nanojunction. This is a new compartment positioned in the bulk cytosol. I then added the process NAADP-induced calcium release to the model and modelled each of the four possible mechanisms that may result in the increased calcium transient amplitude and SR calcium load, observed in the experiments of Capel et al. (2015).

4.1. Defining the nanojunction

Studies have shown that lysosomes are in close contact with the SR (Capel et al., 2015). This small space is called the nanojunction. To add this compartment to the model, its volume has to be defined. The distance between lysosomes and the SR is approximately 25 nm, but the radii and number of lysosomes per cell differ a lot. Fameli et al. (2014) counted 60 to 100 lysosomes in smooth muscle cells. These lysosomes had radii around 200 nm. With these values, I estimate the nanojunctional volume, V_{NJ}, to be 10^{-15} L.

Ions can freely diffuse between the compartments. The diffusion constants for diffusion between the junction, SL and bulk have been determined by Grandi et al. (2011). The nanojunction is placed in the bulk cytosol, so diffusion between these compartments has to be defined. I have decided to let the diffusion constant D_{NJbulk} equal 10^{-14} L/ms. This constant ensures that the nanojunctional calcium concentration approximately equals the concentration in the bulk cytosol under normal circumstances, but when NAADP-induced calcium release is initiated, the increasing nanojunctional calcium concentration does not directly increase the concentration in the bulk cytosol by diffusion.

I have chosen not to buffer the calcium ions in the nanojunction. There is no concrete information about the presence of calcium buffering molecules in this compartment and since the space is very small, there probably is not much buffering activity. In addition, including buffers will just change other parameters, like k_t, which is fitted to the maximal nanojunctional calcium concentration after lysosomal calcium release. This parameter is also linked to the nanojunctional volume. Overall, the parameters that define the nanojunction are closely related.

4.2. Lysosomal calcium release

Lysosomes release calcium into the nanojunction upon β-adrenergic stimulation. The exact detail of the pathway by which NAADP is produced is neglected, both because this is insufficiently known and as the other compounds do not play a further role in the dynamics. Therefore, I have modelled β-adrenoceptor stimulation by an NAADP pulse. The NAADP concentration rises fast and remains constant during some time interval. It then decreases again.

The dynamics of TPC2 have been modelled by Penny et al. (2014). Their model describes NAADP-induced calcium release in skeletal muscle cells. The model is based on data from Pitt et al. (2010), who have found that only limited amounts of NAADP can open TPC2. Since calcium release from lysosomes upon TPC2 activation is very small, the lysosomal calcium concentration is assumed to stay constant. The NAADP-induced calcium flux from the lysosome to the nanojunction is given by

$$I_{lys} = k_t P_{oTPC}(C_L - Ca_{nj}),$$

whereby k_t is a parameter related to the density of the TPC2s, P_{oTPC} is the open probability of TPC2, which depends on the concentration of NAADP, $C_L = 0.5$ mM is the lysosomal calcium concentration, and Ca_{nj} is the nanojunctional calcium concentration, which is dynamic.

Unlike RyR, the dynamics of TPC2 are not described by a system of differential equations. This is due to the fact that the mechanism of RyR is well known while the mechanism of TPC2 is yet be to discovered. Instead, the relation between the concentration of NAADP and the open probability of TPC2 is fitted to data of Pitt et al. (2010). They have found that the relation between log(NAADP) and the open probability of TPC2 is bell-shaped. The optimal NAADP concentration is 23 nM and this results in an open probability of 0.014. I have modelled this by the log-Gaussian function

$$P_{oTPC} = 0.014 \exp\left(-\frac{[\log(NAADP) - \log(23)]^2}{2 \cdot 1.5^2}\right).$$

I have chosen a standard deviation of 1.5, since this fits the data of Pitt et al. (2010) best. Figure 4.1 shows the relation between NAADP and P_{oTPC}.

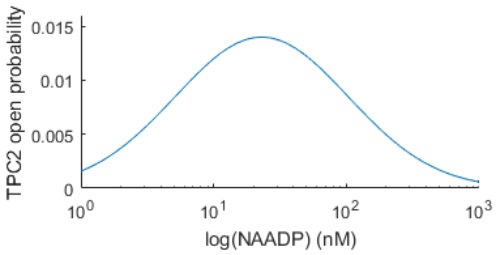

Figure 4.1.: The dependence of the open probability of TPC2 on NAADP.

The parameter k_t was estimated by Penny et al. (2014) using their model. Since I use a different model, I have estimated k_t such that my model gives the same maximal calcium concentration, around 0.7 μM, when the concentration of NAADP is optimal. This yields $k_t = 3.5 \cdot 10^{-16}$ L/ms.

The differential equation for the nanojunctional calcium concentration can now be defined as

$$\frac{dCa_{nj}}{dt} = \frac{D_{NJbulk}}{V_{NJ}} (Ca_i - Ca_{nj}) + \frac{I_{lys}}{V_{NJ}}.$$

Since calcium can diffuse between the nanojunction and the bulk cytosol, the equation for the calcium concentration in the bulk cytosol becomes

$$\frac{dCa_i}{dt} = -J_{SERCA} \frac{V_{SR}}{V_{bulk}} + \frac{D_{SLbulk}}{V_{bulk}}(Ca_{SL} - Ca_i) + \frac{D_{NJbulk}}{V_{bulk}} (Ca_{nj} - Ca_i) - J_{Bbulk}.$$

4.3. CaMKII dynamics

In the Hund-Rudy dynamic cell model for ventricular myocytes, CaMKII phosphorylates certain substances (Hund and Rudy, 2004). I have used their description of the dynamics of CaMKII, but I assume that CaMKII is activated by nanojunctional calcium, instead of calcium in the bulk cytosol.

CaMKII can be in an inactive, bound or trapped state. The state of CaMKII depends on the calcium concentration in the nanojunction. When calcium binds to inactive CaMKII, the kinase transits to the bound state ($CaMK_b$). This is described by

$$CaMK_b = CaMK_{ss} (1 - CaMK_t) \frac{Ca_{nj}}{K_{mCa} + Ca_{nj}}, \tag{4.1}$$

where $CaMK_{ss} = 0.05$ is the fraction of active CaMKII in steady state, and $K_{mCa} = 0.0015$ mM is the calcium concentration where the fraction of bound CaMKII is half-maximal. Bound CaMKII can become trapped ($CaMK_t$) when it is phosphorylated by another bound or trapped CaMKII protein. This happens with rate $\alpha_{CaMK} = 0.05$ ms^{-1}. Trapped CaMKII becomes inactive at constant rate $\beta_{CaMK} = 6.8 \cdot 10^{-4}$ ms^{-1}. This is described by the differential equation

$$\frac{dCaMK_t}{dt} = \alpha_{CaMK} \, CaMK_b \, (CaMK_b + CaMK_t) - \beta_{CaMK} \, CaMK_t.$$

When CaMKII is in the bound or trapped state, it is active ($CaMK_a$), so

$$CaMK_a = CaMK_b + CaMK_t. \tag{4.2}$$

Active CaMKII can phosphorylate certain substances.

The nanojunctional calcium concentration fluctuates around $3.5 \cdot 10^{-4}$ mM. Figure 4.2 shows that $CaMK_a$ is sensitive for small changes in low values of Ca_{nj}. The effect of calcium on the activity of CaMKII can be raised by decreasing the half-maximal constant K_{mCa}. Then the maximal activity of CaMKII is reached for a lower calcium concentration and the slope increases.

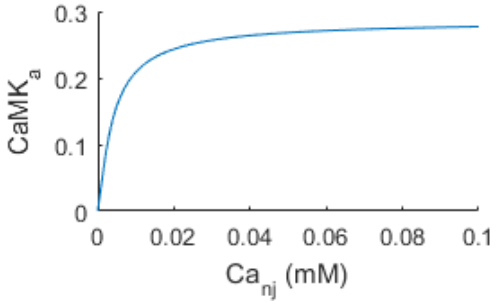

Figure 4.2.: The fraction of active CaMKII against the nanojunctional calcium concentration.

4.4. Models describing the four possible mechanisms

The calcium transient amplitude and SR calcium load increase after β-adrenergic stimulation. It is possible that nanojunctional calcium directly influences SERCA or RyR, but the protein CaMKII could also be involved. CaMKII could be activated by nanojunctional calcium and could phosphorylate SERCA or RyR. This gives rise to four possible mechanisms, which I have modelled all.

4.4.1. Nanojunctional calcium directly influences SERCA or RyR

Only a few things have to be changed to let SERCA and RyR depend on the nanojunctional calcium concentration instead of the calcium concentration in the bulk cytosol and junction respectively. For SERCA this means replacement of Ca_i by Ca_{nj} in Equation 3.6. This does not change the dynamics of SERCA under normal circumstances, since Ca_{nj} then equals Ca_i.

This change cannot be made to let RyR depend on the nanojunctional calcium concentration, since RyR must remain dependent on the junctional calcium concentration. Due to membrane depolarisation, L-type channels open and calcium is transported into the junction, where it binds to RyRs. This is the trigger that initiates the whole contraction process. Without it nothing happens. Under normal circumstances, the calcium concentrations in the bulk cytosol and nanojunction are equal, since calcium can freely diffuse through the compartments. But when calcium is released from lysosomes, the

nanojunctional calcium concentration increases. This does not directly affect the calcium concentration in the bulk cytosol. Hence, by replacing Ca_j with $Ca_j + Ca_{nj} - Ca_i$ in Equations 3.7, RyR becomes dependent on the change in the nanojunctional calcium concentration after calcium is released from lysosomes, while nothing changes under normal conditions.

4.4.2. CaMKII phosphorylates SERCA or RyR

Phosphorylation of SERCA by CaMKII has been modelled by Hund and Rudy (2004). It is assumed that SERCA is bound by PLB. Phosphorylation of PLB increases the activity of SERCA. This is modelled by increasing $V_{maxSERCA}$ in Equation 3.6. The dependence of $V_{maxSERCA}$ on CaMKII is adjusted to produce a maximal increase of 75%, as has been experimentally measured. The factor of increase due to phosphorylation is described by the equation

$$F_{phos} = 0.75 \, \frac{CaMK_a}{K_{mCaMKa} + CaMK_a}, \tag{4.3}$$

whereby $K_{mCaMKa} = 0.15$ mM is the half-maximal constant and $CaMK_a$ is the fraction of active CaMKII, which is dynamic and described by Equation 4.2.

The calcium flux through SERCA can now be redefined as

$$J_{SERCA} = (1 + F_{phos}) \, V_{max_{SERCA}} \, \frac{\left(\frac{Ca_i}{Km_f}\right)^H - \left(\frac{Ca_{SR}}{Km_r}\right)^H}{1 + \left(\frac{Ca_i}{Km_f}\right)^H + \left(\frac{Ca_{SR}}{Km_r}\right)^H}.$$

Higher values of $CaMK_a$ increase J_{SERCA}, as can be seen in Figure 4.3, but this increase is small. The magnitude of this increase is determined by the half-maximal constants K_{mCa} in Equation 4.1 and K_{mCaMKa} in Equation 4.3. Decreasing K_{mCa} results in a higher fraction of active CaMKII for lower nanojunctional calcium concentrations, which raises F_{phos}. Decreasing K_{mCaMKa} increases the slope of F_{phos}. As a consequence, its maximal value is reached for a lower fraction of active CaMKII.

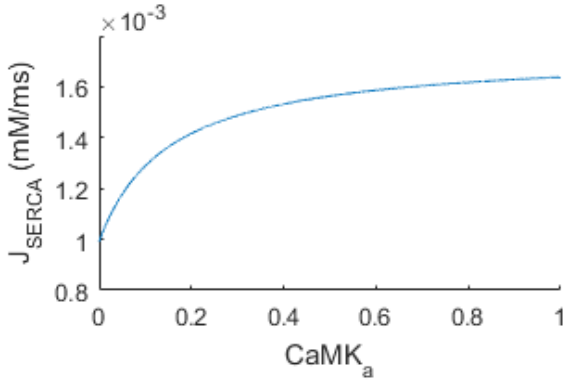

Figure 4.3.: The calcium flux through SERCA against the fraction of active CaMKII.

Hashambhoy et al. (2010) have modelled phosphorylation of RyR by CaMKII by defining phosphorylated states for RyR. Originally, RyR can be in state R, O, I or RI, as is described by Equations 3.7. Each state can be phosphorylated by $CaMK_a$, resulting in the eight-state model

$$
\begin{aligned}
RI &= 1 - R - O - I - R_p - O_p - I_p - RI_p, \\
\frac{dR}{dt} &= (ki_m RI - ki_{SR_{Ca}} Ca_j R) - (ko_{SR_{Ca}} {Ca_j}^2 R - ko_m O) - (k_p CaMK_a R - k_d R_p), \\
\frac{dO}{dt} &= (ko_{SR_{Ca}} {Ca_j}^2 R - ko_m O) - (ki_{SR_{Ca}} Ca_j O - ki_m I) - (k_p CaMK_a O - k_d O_p), \\
\frac{dI}{dt} &= (ki_{SR_{Ca}} Ca_j O - ki_m I) - (ko_m I - ko_{SR_{Ca}} {Ca_j}^2 RI) - (k_p CaMK_a I - k_d I_p), \\
\frac{dRI_p}{dt} &= (ko_m I_p - ko_{SR_{Ca}} {Ca_j}^2 {Ca_{shift}}^2 RI_p) - (ki_m RI_p - ki_{SR_{Ca}} Ca_j R_p) + (k_p CaMK_a RI - k_d RI_p), \\
\frac{dR_p}{dt} &= (ki_m RI_p - ki_{SR_{Ca}} Ca_j R_p) - (ko_{SR_{Ca}} {Ca_j}^2 {Ca_{shift}}^2 R_p - ko_m O_p) + (k_p CaMK_a R - k_d R_p), \\
\frac{dO_p}{dt} &= (ko_{SR_{Ca}} {Ca_j}^2 {Ca_{shift}}^2 R_p - ko_m O_p) - (ki_{SR_{Ca}} Ca_j O_p - ki_m I_p) + (k_p CaMK_a O - k_d O_p), \\
\frac{dI_p}{dt} &= (ki_{SR_{Ca}} Ca_j O_p - ki_m I_p) - (ko_m I_p - ko_{SR_{Ca}} {Ca_j}^2 {Ca_{shift}}^2 RI_p) + (k_p CaMK_a I - k_d I_p).
\end{aligned}
$$

States are phosphorylated and dephosphorylated with rate k_p and k_d respectively. The parameter $k_p = 2.38 \cdot 10^{-4}$ ms^{-1} was experimentally measured. I have estimated k_d and Ca_{shift} such that 24% of the states are phosphorylated and the open probability $O + O_p$ increases 129% in steady state, with respect to the unphosphorylated model for RyR. This yields $k_d = 1.36e - 5$ ms^{-1} and $Ca_{shift} = 9$.

The steady state equations can still be calculated analytically, but have become very long and complicated. Figure 4.4 illustrates the dependence of the open probability of RyR on the fraction of CaMKII in the active state. Normally this fraction fluctuates around 0.02, hence a small increase in CaMKII activity will result in a significantly higher open probability. This sensitivity can further be increased by increasing k_p or decreasing k_d. The other parameters change the maximal open probability of RyR.

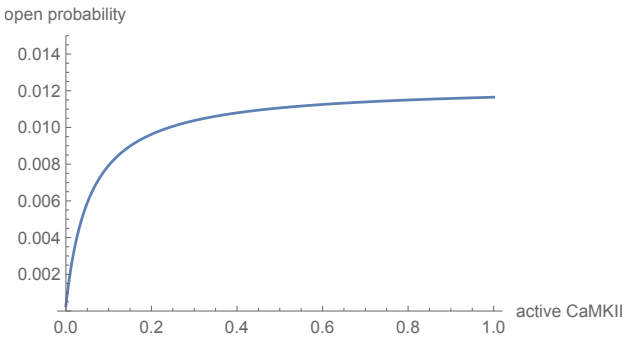

Figure 4.4.: The open probability of RyR against the fraction of active CaMKII.

5. Results

Results are generated for each of the four possible models described in the previous chapter. It has been demonstrated that the amplitude of the calcium transient, as well as the SR calcium load, increases upon β-adrenergic stimulation. Data from the Terrar laboratory, University of Oxford (L. Elson, DPhli thesis, 2009), show an increase of 38 $\pm$ 6% in the contraction amplitude, 15 seconds after rapidly adding 60 nM NAADP-AM to he myocyte. This is shown in Figure A.1. It is reasonable to assume that this means an increase of 38 $\pm$ 8% in the calcium transient amplitude. Collins et al. (2011) have found an increase of 31 $\pm$ 8 % in SR load after having added 60 nM NAADP-AM for two minutes, as can be seen in Figure A.2.

I generated my results by increasing the NAADP concentration to 60 nM at $t = 30$ s. This concentration is maintained for two minutes. The NAADP pulse and its effects on the nanojunctional calcium concentration and the fraction of active CaMKII can be seen in Figure 5.1. The nanojunctional calcium concentration increases 36% and this results in an increase of 156% in the fraction of active CaMKII.

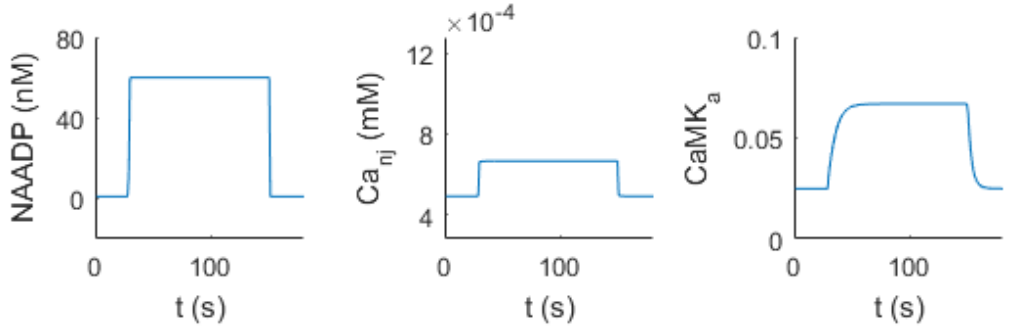

Figure 5.1.: The simulated NAADP pulse and its effect on the nanojunctional calcium concentration and the fraction of active CaMKII.

5.1. Nanojunctional calcium directly influences SERCA

In the model where SERCA is dependent on nanojunctional calcium, the calcium transient amplitude and SR load increase during β-adrenergic stimulation, as can be seen in Figure 5.2. The SR takes up more calcium, thereby increasing ko_{SRCa} and decreasing ki_{SRCa}, which are described by Equations 3.8. This results in a higher open probability for RyR. As a consequence, the SR releases more calcium into the junction and the calcium transient increases. The system rapidly reaches a new steady state and returns to its original steady state when the NAADP pulse ends.

Twenty seconds after the NAADP pulse started, a new steady state is reached. The calcium transient amplitude has increased 47%. This is higher than the observed increase of 38%. In comparison, the SR load has only increased 12%, where 31% has been observed. To obtain an increase in the calcium transient amplitude of 38%, the volume of the nanojunction can be increased by factor 1.5. This results in less increase of the nanojunctional calcium concentration during β-adrenergic stimulation. However, this also decreases the SR load, which is already lower than has been measured. The SR load can be raised by increasing $V_{maxSERCA}$ or decreasing Km_f, but this drastically changes the dynamics of the myocyte under normal circumstances. In addition, this will also further increase the calcium transient amplitude.

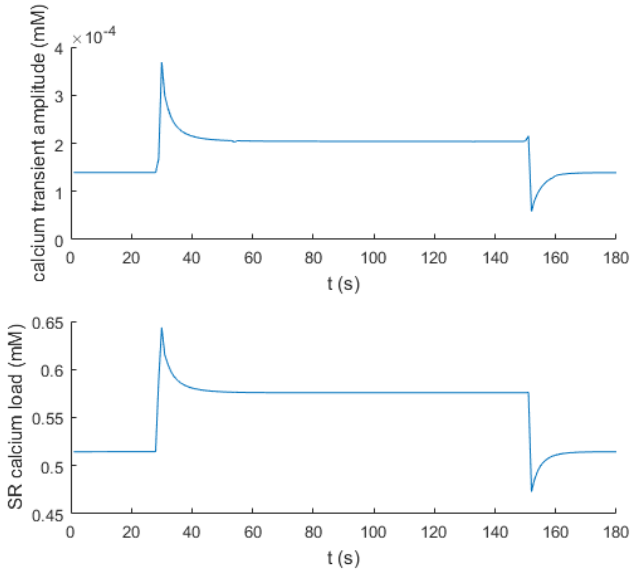

Figure 5.2.: The calcium transient amplitude and SR calcium load when SERCA is dependent on the nanojunctional calcium concentration. The 60 nM NAADP pulse starts at t = 30 s and ends at t = 150 s.

5.2. Nanojunctional calcium directly influences RyR

Dependence of RyR on the nanojunctional calcium concentration results in a decrease in the calcium transient amplitude upon β-adrenergic stimulation, as can be seen in Figure 5.3. Due to a lower calcium concentration in the bulk cytosol, the activity of SERCA also decreases, resulting in a slightly decreased SR calcium load. Apparently, the calcium released from lysosomes on top of the calcium entering through L-type channels, raises the junctional calcium concentration above the point where the RyR open probability starts to decrease. This can be seen in Figure 3.5. This point can be raised by decreasing ko_{SRCa} and increasing ko_m. By decreasing ko_{SRCa} 100 times or increasing ko_m 40 times, the open probability of RyR increases during the NAADP pulse, raising the calcium transient amplitude. But the SR load still decreases. It seems that calcium uptake by SERCA does not weigh up against the increased release by RyR.

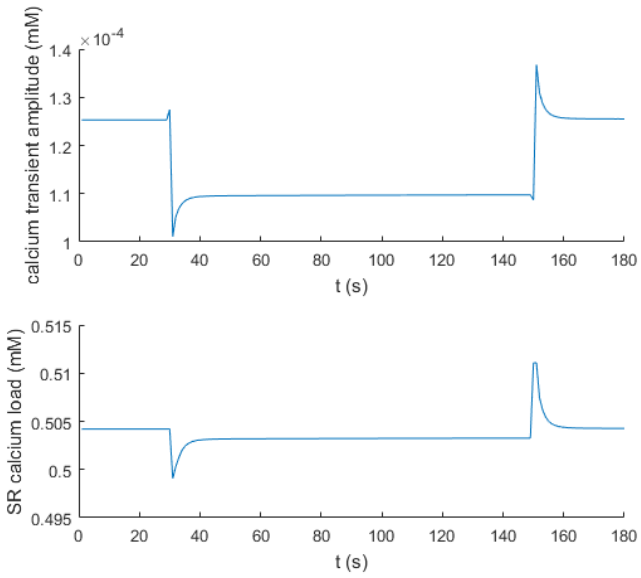

Figure 5.3.: The calcium transient amplitude and SR calcium load when RyR is dependent on the nanojunctional calcium concentration. The 60 nM NAADP pulse starts at t = 30 s and ends at t = 150 s.

5.3. CaMKII phosphorylates SERCA

Figure 5.4 shows a small increase in the calcium transient amplitude and SR calcium load, when SERCA is phosphorylated by CaMKII. The rise in nanojunctional calcium has increased the activity of CaMKII, resulting in a higher activity of SERCA. This leads to an increase of 0.8% in the SR calcium load. As a consequence, the calcium transient amplitude increases 2.2%.

Clearly, phosphorylation by CaMKII does not activate SERCA enough to obtain an increase in the calcium transient amplitude and SR calcium load of 38% and 31% respectively. Decreasing K_{mCa} in Equation 4.1 raises the sensitivity of CaMKII for nanojunctional calcium. Hence, this results in a higher fraction of active CaMKII upon β-adrenergic stimulation. But this fraction also increases under normal conditions. As a consequence, β-adrenergic stimulation does not increase the CaMKII activity more than before. In addition, Figure 4.3 shows that the increase in J_{SERCA} is relatively small when $CaMK_a$ rises. The same accounts for decreasing the parameter K_{mCaMKa} in Equation 4.3. The optimal choice is $K_{mCa} = 0.0011$ mM and $K_{mCaMKa} = 0.083$ mM. With these values the difference in CaMKII activity and F_{phos} under normal circumstances and during β-adrenergic stimulation is maximal. But this does not change the calcium transient amplitude and SR calcium load significantly.

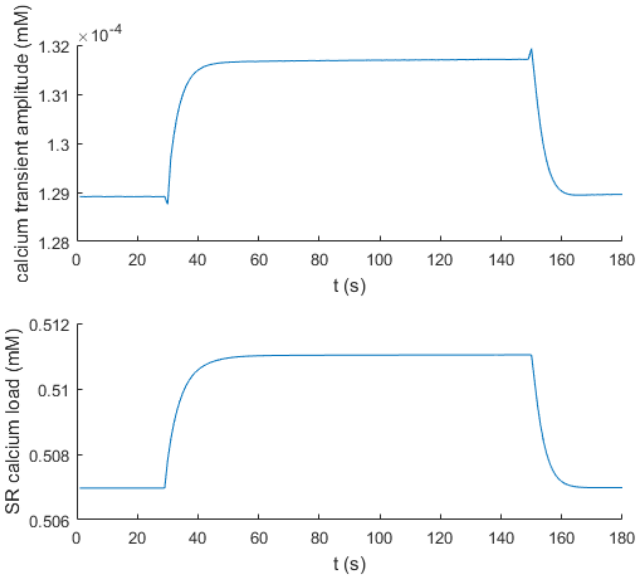

Figure 5.4.: The calcium transient amplitude and SR calcium load when SERCA is phosphorylated by CaMKII. The 60 nM NAADP pulse starts at t = 30 s and ends at t = 150 s.

5.4. CaMKII phosphorylates RyR

In the model where RyR is phosphorylated by CaMKII, the open probability of RyR increases upon β-adrenergic stimulation. It can be deduced from Figure 5.5 that this results in a decreasing SR calcium load. Calcium uptake by SERCA clearly does not weigh up against the increased release by RyR. At first, this results in an increase in the calcium transient of 3%, but then ko_{SRCa} decreases and ki_{SRCa} increases, due to the extremely decreased SR load. This has been described by Equations 3.8. As a consequence, the open probability of RyR decreases, resulting in a decreasing calcium transient amplitude.

I have also combined phosphorylation of RyR with phosphorylation of SERCA, but this does not change the results pictured in Figure 5.5. The effect of CaMKII on SERCA is too weak to lead to a significant increase in the SR calcium load.

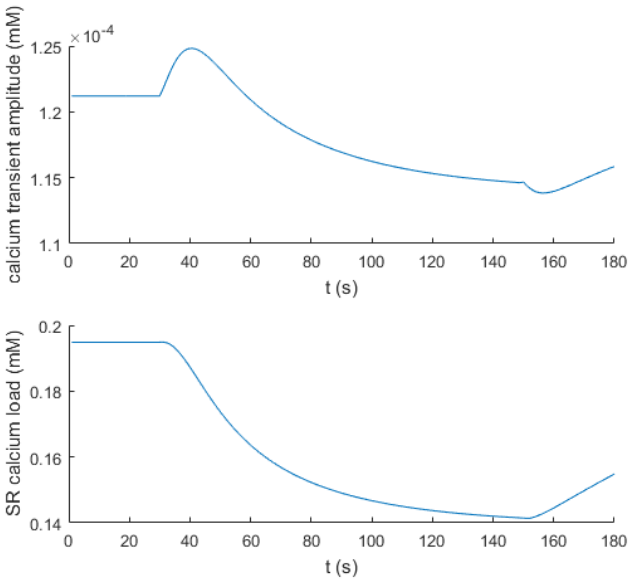

Figure 5.5.: The calcium transient amplitude and SR calcium load when RyR is phosphorylated by CaMKII. The 60 nM NAADP pulse starts at t = 30 s and ends at t = 150 s.

6. Discussion

Stimulation of the β-adrenoceptor leads to NAADP-induced calcium release. Data from the Terrar Laboratory at the University of Oxford and Collins et al. (2011) suggest an increase in calcium transient amplitude and SR calcium load during this process. The mathematical model developed in this thesis simulates NAADP-induced calcium release and the four potential mechanisms that could cause these results.

Dependence of SERCA on the nanojunctional calcium concentration has great effect on the calcium transient amplitude and also increases the SR calcium load during β-adrenergic stimulation. However, the simulated SR load increases 12% while an increase of 31% was experimentally measured. The observed increase of the calcium transient amplitude can be simulated by increasing the nanojunctional volume in the model, but this also decreases the SR calcium load. Nevertheless, it is likely that this mechanism is involved.

The possibility that nanojunctional calcium directly influences RyR can be ruled out, since this decreases the calcium transient amplitude and SR calcium load. For the same reason, it can be rejected that activated CaMKII only phosphorylates RyR. RyR could be involved in combination with SERCA, but amplification of RyR will always lead to a decreasing SR load. If this is the case, the activity of SERCA must be high enough to overcome this decrease.

It has been demonstrated by Capel et al. (2015) that the calcium transient amplitude and SR calcium load do not increase upon application of NAADP when CaMKII is inhibited. Hence phosphorylation of SERCA by CaMKII is the most logic option. However, the model produces a very small increase in calcium transient and SR calcium load. These results cannot be changed by altering parameters, since this also leads to higher activity of CaMKII and SERCA under normal circumstances.

It can be concluded that SERCA is a better target for NAADP-induced calcium release than RyR, and hence the focus should be on SERCA. It is likely that CaMKII is involved in increasing the calcium transient and SR load, but at this point the simulations of the model where CaMKII phosphorylates SERCA do not resemble the data. It could be the case that CaMKII is involved in some other way, for example by activating another substance that then raises the activity of SERCA. This substance must have low activity under normal circumstances and become highly active upon activation by CaMKII. Nevertheless, the next step is to improve the model for phosphorylation of SERCA by CaMKII.

The data in Figure A.1 and Figure A.2 were generated by placing the myocyte in a solution of 60 nM NAADP-AM. This is different from raising the NAADP concentration in the cell to 60 nM, as I have done to simulate the results. The -AM part of the molecule is always being chopped off inside the cell. This results in a gradient forcing NAADP-AM into the cell and therefore the actual concentrations reached inside the cell may be much higher than those outside the cell. Nevertheless, the exact concentration of NAADP that is reached inside the cell during these experiments is unknown. In the model, a higher NAADP pulse leads to less effect on the calcium transient amplitude and SR calcium load. This can be explained by the definition of the open probability of TPC2, which is maximal for 23 nM NAADP, as can be seen in Figure 4.1.

The model for NAADP-induced calcium release is well validated to data of Pitt et al. (2010). The parameters V_{NJ}, D_{NJbulk} and k_t are fitted such that the nanojunctional calcium concentration equals 0.7 μM upon optimal β-adrenergic stimulation. But the dynamics of CaMKII can be questioned. The parameters in the equations that describe the dynamics of CaMKII are experimentally measured and are not fitted to the model I have constructed. The same accounts for the phosphorylation of SERCA by CaMKII. Maximal activities have been defined, but in the simulations these are not reached by far. By way of contrast, the dynamics of phosphorylated RyR have been altered such that the open probability and phosphorylation fraction in my model agree with experimental data. It is noteworthy that the effects of CaMKII on RyR are significant, in contrast to the effects on SERCA. More research is required to improve the model for the phosphorylation of SERCA by CaMKII.

The model contributes to the understanding of NAADP-induced calcium release and its effects. Theories have been ruled out and new questions have been raised. In future studies, the focus should be on the effect of NAADP-induced calcium release on SERCA. The model has also provided new ideas for biomedical experiments. Additional research, biomedical as well as mathematical, is needed to understand the effects of NAADP-induced calcium release and ultimately cure atrial fibrillation.

Acknowledgements

I would like to thank everyone who has supported me during my bachelor studies. My thanks go out to lecturers of the Vrije Universiteit Amsterdam, my fellow students, friends and family. In particular, I would like to thank my supervisor Dr. Robert Planqué for providing me this great subject for my thesis and guiding me through this project. Our conversations really helped me structure my thoughts. I would also like to thank Dr. Rebecca A. Capel and Dr. Rebecca B. Burton for involving me in their research and providing me with information. Their advice has been of great help. I really enjoyed our collaboration and I am happy to have been part of this investigation.

References

[1] Aarhus R, Graeff RM, Dickey DM, Walseth TF, Lee HC. 1995. ADP-ribosyl cyclase and CD38 catalyze the synthesis of a calcium-mobilizing metabolite from NADP. *The Journal of Biological Chemistry*. **270**:30327-33.

[2] Bayliss RA, Bolton EL, Bloor-Young D, Churchill G, Galione A, Terrar DA. 2012. Interfering with lysosomal function in atrial and ventricular myocytes reduces the response to isoprenaline. *Proceedings of the Physiological Society*. **28**:C10 and PC10.

[3] Bruggeman FJ. 2014. *Introduction to Systems Biology* [Syllabus]. Vrije Universiteit Amsterdam.

[4] Calcraft PJ, Ruas M, Pan Z, Cheng X, Arredouani A, Hao X, Tang J, Rietdorf K, Teboul L, Chuang KT, Lin P, Xiao R, Wang C, Zhu Y, Lin Y, Wyatt CN, Parrington J, Ma J, Evans AM, Galione A, Zhu MX. 2009. NAADP mobilizes calcium from acidic organelles through two-pore channels. *Nature*. **459**:596-600.

[5] Capel RA, Bolton EL, Lin WK, Aston D, Wang Y, Liu W, Wang X, Burton RB, Bloor-Young D, Shade K, Ruas M, Parrington J, Churchill GC, Lei M, Galione A, Terrar DA. 2015. TPC2 and NAADP enhance cardiac β-adrenoceptor signaling. *The Journal of Biological Chemistry*. **290**:30087-98.

[6] Collins TP, Bayliss R, Churchill GC, Galione A, Terrar DA. 2011. NAADP influences excitation-contraction coupling by releasing calcium from lysosomes in atrial myocytes. *Cell Calcium*. **50**:449-58.

[7] Diekmann O, Planqué R. *Mathematical Biology* [Syllabus]. Vrije Universiteit Amsterdam.

[8] Fameli N, Ogunbayo OA, van Breemen C, Evans AM. 2014. Cytoplasmic nanojunctions between lysosomes and sarcoplasmic reticulum are required for specific calcium signaling. *F1000Research*. **3**:93.

[9] Grandi E, Pandit SV, Voigt N, Workman AJ, Dobrev D, Jalife J, Bers DM. 2011. Human Atrial Action Potential and Ca^{2+} Model: Sinus Rhythm and Chronic Atrial Fibrillation. *Circulation Research*. **109**:1055-66.

[10] Hashambhoy YL, Greenstein JL, Winslow RL. 2010. Role of CaMKII in RyR leak, EC Coupling and Action Potential Duration: A Computational Model. *Journal of Molecular and Cellular Cardiology*. **49**:617-24.

[11] Helle SC, Kanfer G, Kolar K, Lang A, Michel AH, Kornmann B. 2013. Organization and function of membrane contact sites. *Biochimica et Biophysica Acta*. **1833**:2526-41.

[12] Hund TJ, Rudy Y. 2004. Rate Dependence and Regulation of Action Potential and Calcium Transient in a Canine Cardiac Ventricular Cell Model. *Circulation*. **110**:3168-74.

[13] Keener J, Sneyd J. 2009. *Mathematical Psysiology I: Cellular Physiology*. New York: Springer Science+Business Media.

[14] Penny CJ, Kilpatrick BS, Min Han J, Sneyd J, Patel S. 2014. A computational model of lysosome-ER Ca^{2+} microdomains. *Journal of Cell Science*. **127**:2934-43.

[15] Pitt SJ, Funnell TM, Sitsapesan M, Venturi E, Rietdorf K, Ruas M, Ganesan A, Gosain R, Churchill GC, Zhu MX, Parrington J, Galione A, Sitsapesan R. 2010. TPC2 is a novel NAADP-sensitive Ca^{2+} release channel, operating as a dual sensor of luminal pH and Ca^{2+}. *The Journal of Biological Chemistry*. **285**:35039-46.

[16] Shannon TR, Wang F, Puglisi J, Weber C, Bers DM. 2004. A Mathematical Treatment of Integrated Ca Dynamics within the Ventricular Myocyte. *Biophysical Journal*. **87**:3351-71.

[17] Weiss JN. 1997. The Hill equation revisited: uses and misuses. *The FASEB Journal*. **11**:835-41.

A. Data

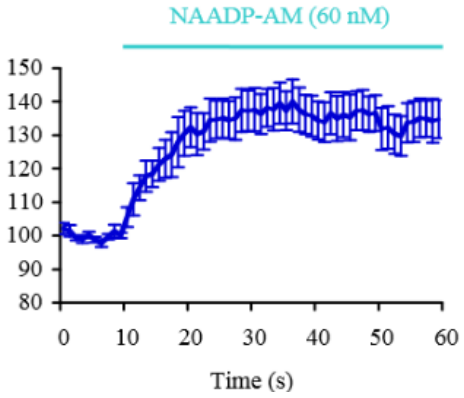

Figure A.1.: Data from the Terrar laboratory, University of Oxford (L. Elson, DPhli thesis, 2009). The effect of 60 nM NAADP-AM on the mean amplitudes of guinea-pig ventricular myocyte contractions. A rapid switch to 60 nM NAADP-AM was made at 10 s. This resulted an increase in contraction amplitude of 38±6% at 25 s.

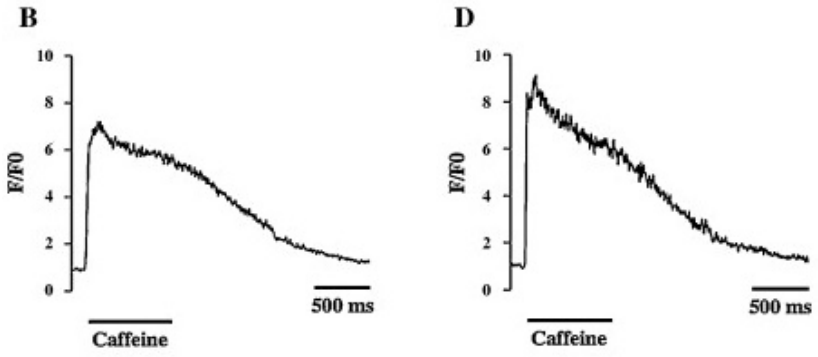

Figure A.2.: Figures B and D from Figure 6 of Collins et al. (2011) show the SR load in fluorescence level F/F0. Atrial myocytes were stimulated with caffeine to release all calcium from the SR. Figure D shows the estimated SR load of myocytes that have first been stimulated with 60 nM NAADP-AM for two minutes. This resulted in an increase in SR load of 31±8%.